A TWO DIMENSIONAL FINITE DIFFERENCE TIME DOMAIN ANALYSIS OF THE QUIET ZONE FIELDS OF AN ANECHOIC CHAMBER

Final Report
Contract number: NASA NAG 1-1221

submitted to

Dr. Fred Beck
NASA Langley Research Center
Mail Stop 490
Hampton, VA 23665

submitted by

Deirdre A. Ryan, Raymond J. Luebbers, Truong X. Nguyen*,
Karl S. Kunz and David J. Steich

Department of Electrical and Computer Engineering
The Pennsylvania State University
University Park, PA 16802
(814) 865-2362/865-2776

*Research Triangle Institute
Hampton, VA 23665

January 1992

A TWO DIMENSIONAL FINITE DIFFERENCE TIME DOMAIN ANALYSIS OF THE QUIET ZONE FIELDS OF AN ANECHOIC CHAMBER

by

Deirdre A. Ryan, Raymond J. Luebbers, Truong X. Nguyen*,
Karl S. Kunz, and David J. Steich

Electrical and Computer Engineering Department
The Pennsylvania State University
University Park, PA., 16802

*Research Triangle Institute
Hampton, VA., 23665

January 1992

Abstract

Prediction of anechoic chamber performance is a difficult problem. Electromagnetic anechoic chambers exist for a wide range of frequencies but are typically very large when measured in wavelengths. Three dimensional Finite Difference Time Domain (FDTD) modeling of anechoic chambers is possible with current computers but at frequencies lower than most chamber design frequencies. However, two dimensional FDTD (2D-FDTD) modeling enables much greater detail at higher frequencies and offers significant insight into compact anechoic chamber design and performance.

A major subsystem of an anechoic chamber for which computational electromagnetic analyses exist is the reflector. First, this paper presents an analysis of the quiet zone fields of a low frequency anechoic chamber produced by a uniform line source

and a reflector in two dimensions using the FDTD method. The 2D-FDTD results are compared with results from a three dimensional corrected Physical Optics calculation and show good agreement. Next, a directional source is substituted for the uniform radiator. Finally a two dimensional anechoic chamber geometry including absoring materials is considered, and the 2D-FDTD results for these geometries appear reasonable.

Introduction

The Finite Difference Time Domain (FDTD) method has seen growing interest as a means for solving problems involving electromagnetic interactions with general materials and shapes. The Finite Difference Time Domain method uses finite differences to approximate both spatial and temporal derivatives to directly solve Maxwell's curl equations. The computational space is divided into cells and the constitutive parameters for each cell are specified. An excitation source is specified and the electromagnetic fields are marched in time through the computation space. Fields, currents, power flow, or other quantities of interest are available at each time step. The particular method applied here is based on the Yee algorithm [1]. The cells are rectangular and are required to be a small fraction of the smallest wavelength under consideration. The FDTD literature is quite extensive and [2] - [6] represent recent general information on the topic.

The volume which can be modeled using FDTD is limited by computer resources. On a work station, a reasonable size might be 500,000 cubical cells. At a constraint of 10 cells per wavelength, this would allow for modeling a space about 8 wavelengths on a side. This is much smaller than most anechoic chambers. However, low frequency chambers exist in this size range, and the fields in a 100 MHz four wire chamber were modeled in three dimensions using FDTD [7]. If supercomputers are considered, the available modeling space may be increased. The FDTD method is well suited to highly parallel machines. For a large version of such a machine, calculating the fields through a space of 4 million cells can be done for enough time steps to observe the important interactions in approximately 2 hours [8]. With a problem space size of 4 million cells and a constraint of 10 cells per wavelength, a space about 16 wavelengths on a side can be modeled. While this is a significant increase, it is still much smaller than most anechoic chambers. Thus, at present, three dimensional modeling of a complete anechoic chamber using FDTD is limited to low frequencies, pending the next generation of supercomputers.

Since three dimensional modeling of anechoic chambers is not feasible at the present time using FDTD (except at low frequencies), we consider two dimensional modeling in this paper.

With reasonable computational power and graphics capabilities, one can observe the fields emanate from the source location,

propagate to the reflector, form a localized plane wave, and propagate through the quiet zone. This is not a ray tracing approach, but a full solution of Maxwell's equations. Thus electromagnetic interactions such as diffraction from the reflector edge and reflections from imperfect absorbing materials are included in the calculations.

Since the computations are performed directly in the time domain, techniques used in chamber operation, such as range gating to eliminate unwanted reflections, can be directly simulated.

The time response of the fields at any cell or set of cells in the computational space may be saved and processed at a later time with Fast Fourier Transforms to provide frequency domain results for such quantities as magnitude and phase ripple across the quiet zone as a function of frequency or as a function of position at any number of frequencies. Thus, within the limitations described above, the FDTD technique is well suited to analyzing anechoic chamber geometries.

Two Dimensional Finite Difference Time Domain (2D-FDTD)

The following two dimensional approach is similar to the three dimensional FDTD method with the standard modifications of Maxwell's curl equations. The two dimensional analysis assumes

invariance in one direction, and we choose the z direction, arbitrarily. Next, to provide shorter run times for the fields of interest, Maxwell's curl equations can be divided into two cases: TM_z (no H_z component) and TE_z (no E_z component). The TM_z equations follow:

$$\frac{\partial E_z}{\partial t} = -\frac{\sigma}{\epsilon} E_z + \frac{1}{\epsilon}\left(\frac{\partial H_y}{\partial x} - \frac{\partial H_x}{\partial y}\right) \tag{1}$$

$$\frac{\partial H_x}{\partial t} = -\frac{1}{\mu}\frac{\partial E_z}{\partial y} \tag{2}$$

$$\frac{\partial H_y}{\partial t} = \frac{1}{\mu}\frac{\partial E_z}{\partial x} \tag{3}$$

Implementing central differences in space and time, Equation (1) becomes

$$\begin{aligned} EZT^{n}(I,J) &= \frac{\epsilon}{\epsilon + \sigma\Delta t} EZT^{n-1}(I,J) \\ &+ \frac{\Delta t}{\Delta x\,(\epsilon + \sigma\Delta t)}\left[HYT^{n-1/2}(I,J) - HYT^{n-1/2}(I-1,J)\right] \\ &- \frac{\Delta t}{\Delta y\,(\epsilon + \sigma\Delta t)}\left[HXT^{n-1/2}(I,J) - HXT^{n-1/2}(I,J-1)\right] \end{aligned} \tag{4}$$

where EZT, HYT, and HXT represent (FORTRAN) computer variables used to store the corresponding field quantities. The TE_z computations use a similar set of three equations. Figure 1 illustrates the

placement of the field components on the 2D-FDTD computational cell.

Having discussed the reduction from three dimensions to two dimensions of Maxwell's curl equations and given an example of the implementation of the 2D-FDTD field equations in the computation, consider in the next section the application of these equations to analyzing the fields of a reflector.

Application of the FDTD Method to Chamber Fields

The desired waveform in the measurement region of an anechoic chamber, commonly called the "quiet zone", is planar. How effectively this plane wave is achieved depends mainly on the design of the reflector and directional source. Various degradations of the waveform occur when spurious signals from the absorber, reflector edge, feed source, etc., destructively interfere with the planar wavefront.

FDTD is a suitable choice for analyzing an anechoic chamber because these effects can be considered separately. First, the quiet zone fields produced by a reflector illuminated by a uniform source are computed. Next, the uniform source is replaced by a directional source and the analysis repeated. Finally, the absorber is included in the calculation. Following is a

description of the chamber components and an outline of the FDTD approach.

The reflector is designed for use in a low frequency anechoic chamber and is illuminated by fields located at the focal point. This particular reflector can be used at frequencies below the frequency determined by the size of the parabolic section because of additional edge treatments. The reflector uses a cosine blending function for blended rolled edge treatments [9]. Since this is a two-dimensional analysis, only the centerline of the reflector is modeled (see Figure 2). The reflector is a perfect electrical conductor and the reflector supports are not modeled.

The three dimensional shapes of the absorber sections (wedges and pyramids) are simulated in two dimensions by spatially tapering the conductivity and permittivity. The pyramidal and wedge absorber are modeled by tapering the conductivity and relative permittivity from the free space values at their tips to higher values of 0.02 Siemens/m and 4.2, respectively, at the bases located along the perfectly conducting wall.

Full anechoic chamber analysis uses the reflecting walls of the anechoic chamber as the computational space boundaries and does not use the customary FDTD absorbing outer boundaries. These FDTD outer boundaries simulate free space and are designed to absorb incident fields in order to prevent a reflection from the problem

space termination. In the full chamber geometry including absorber, the perfectly conducting chamber outer walls form the problem space boundaries and the error associated with free space termination of the computational space is eliminated. However, for the other two geometries, a second order Mur radiating boundary condition on the electric field was imposed [10,11] so that the source and reflector appear to be in an infinite area of free space. Surrounding the reflector and source with free space enabled a comparison of the FDTD method with the corrected Physical Optics method.

The excitation source is located at the focal point of the reflector. For the first geometry considered the excitation is a line source which is infinite in the +z and -z directions. This source uniformly radiates a cylindrical wave. For the second and third geometries a directional source is chosen. This directional source is a two dimensional horn with a 2.0 wavelength aperture. This horn was chosen to provide some directivity to the wave, yet remain unobtrusive to the planar wavefront.

Field values at all cells within the computational space are computed in two dimensions using FDTD. The first geometry requires "time-gating" of the fields in order to isolate the reflected fields. The first fields to enter the quiet zone are due to direct illumination from the line source. At a later time fields enter the quiet zone due to reflection by the reflector and these are of

interest. After the direct radiation from the source clears the quiet zone, the fields are sampled. Therefore, by time-gating the quiet zone signal, only the fields reflected by the reflector are recorded. The duration of the pulse and the size of the quiet zone as well as the distance the reflected wave travels determine the clear time. The other two geometries did not require time-gating since a directional source was used.

The electric field at a position along the length of the chamber and various positions above the floor is sampled in time. The time record at each quiet zone position is then transformed to the frequency domain to determine the magnitude and phase responses versus quiet zone position. An FFT algorithm is used to extract the desired frequency component.

Having discussed the method by which the quiet zone fields are determined, let us analyze the two dimensional chamber illustrated in Figure 3.

FDTD Demonstration

The anechoic chamber illustrated in Figure 3 is designed for use at low frequencies. The centerline of the chamber is shown and is 80 feet (24.4 meters) in the x direction and 48 feet (14.6 meters) in the y direction. The reflector is 26' in diameter and

the focal point of the reflector, denoted by an X in Figure 3, is 45 feet from the back wall and level with the floor. The absorber covers the conducting walls of the chamber and the majority is 4' high. The fields are sampled at X_o = 39.5' and at increments of one foot in the y direction. There are 41 sample locations and several are depicted in Figure 3 by the small dots.

The fields may be sampled at any location in the chamber, but we are interested in the fields in the quiet zone. The sampling location in the X direction is designated by X_o and marks a position in the quiet zone along the length of the chamber. The quiet zone fields at locations from the floor to the ceiling are sampled in time by holding the X position constant and varying the Y position.

The frequency of interest is 330 MHz and twenty cells per wavelength are used to model the chamber, 537 cells in x and 323 cells in y. For the first two FDTD geometries considered, a free space variable cell border (indicated by CB in Figure 4) is added on all sides of the problem space to reduce the reflections from the Mur radiating boundary conditions. A cell border of between 100 and 300 cells was sufficient. The cell size does not depend on the cell border and is determined solely by the chamber dimensions, the frequency of interest, and the number of modeling cells per wavelength. Therefore, the cell size is kept constant at 4.5 cm

and the time step, based on the Courant stability requirement, is 0.1072 ns.

The larger of the two problem spaces considered, 837 by 623 (521,451 cells), is a reasonable size for a workstation and the time required for a computation involving 41 quiet zone locations is approximately 35 minutes on an IBM RS6000 model 320H.

Reflector and Line Source

The first problem space geometry is shown in Figure 4. The chamber dimensions are depicted by the dashed line. The computational space extends beyond the chamber area by CB in all directions and is depicted by the solid line. The line source is located at the focal point (X) of the reflector.

The electromagnetic problem consists of analyzing the quiet zone fields produced by a reflector illuminated by a line source in two dimensions. The excitation source is imposed at the focal point of the reflector and the direct radiation from the source is time-gated out. After the clear time, the electric field across the quiet zone is sampled in time. The time domain results are transformed to the frequency domain for comparison with three dimensional results obtained from a corrected Physical Optics computation.

The time variation for the line source is defined analytically. The analytic function defines a sinusoidal pulse with sinusoidal frequency of 330 MHz. The 330 MHz sine wave is modulated by a Gaussian pulse envelope with a rise time of 16 time steps and a width of 75 time steps. Figure 5 depicts the time variation of the sine and the Gaussian ramping function on the leading and trailing edge of the sinusoidal pulse is evident.

The following example illustrates the need for "time-gating" for the first geometry. The electric field versus time at two locations in the quiet zone is shown in Figures 6 and 7. The first fields to enter the quiet zone are the direct radiation from the source. The second set of fields enter the quiet zone after propagating from the source location to the reflector and from the reflector to the quiet zone. The amount of time required for the direct radiation to propagate out of the quiet zone is based on the time width of the line source and the height of the quiet zone. A clear time of 560 time steps was sufficient. Note the difference in amplitude and the shift in time of the direct radiation in Figures 6 and 7. The sample point in Figure 6 is at X_o = 39.5 and Y = 18 feet. The sample point in Figure 7 is at the same X position but Y = 22 feet above the floor. Therefore, the amplitude of the direct radiation is higher in Figure 6 than in Figure 7 and the direct radiation appears at an earlier time at the closer sampling location. Note also that the amplitude and time placement of the reflected waves in the Figures are virtually identical.

Reflector and Directional Source

The second electromagnetic problem consists of examining the quiet zone fields of the reflector using a two dimensional rectangular horn as the feed antenna. The same line source as above is placed half a wavelength from the feed end of the horn antenna. The horn is positioned so that the focal point of the reflector is in the throat of the horn. Figure 8 shows the horn in detail with the source location marked by a circle and the focal point location marked by an X. The purpose of the horn antenna is to direct the radiation towards the reflector and not distribute it evenly throughout the space as in the line source geometry considered previously. The time domain results are transformed to the frequency domain and compared with the results obtained using the line source radiator.

A Mur second order radiating boundary is also used in this analysis; however, time-gating of the quiet zone fields is not necessary since the horn is a directive source.

This geometry illustrates the effect of a directional source on the quiet zone fields. The horn directs most of the energy toward the center of the reflector. Thus, the reflector is not uniformly illuminated and the quiet zone fields show this effect.

Two Dimensional Chamber Geometry

The third electromagnetic problem consists of examining the quiet zone fields using the two dimensional horn antenna, the reflector, and the absorbing material backed by the chamber walls. The problem setup, depicted in Figure 3, is the same as for the second geometry considered except that the outer boundaries of the problem space are the perfectly conducting chamber walls, which are then covered by the absorber. This geometry illustrates the attenuating effect of the absorber and the quiet zone fields do indeed show this.

Comparison of Results

The results obtained using the FDTD Method for the reflector and line source geometry are compared with results from a three dimensional corrected Physical Optics (PO) approach in Figures 9 - 12. The TM results for the other two geometries considered are also compared (Figures 13 and 14) and illustrate the effect of the directional source and the absorber.

In the corrected PO approach, the fields of the reflector are computed using PO. The end point contributions from the shadow boundary of the reflector surface are subsequently subtracted from the PO solution [12,13]. The PO fields are computed by dividing

the reflector surface into triangular patches 0.07 wavelengths on a side. The first two terms of the infinite series representing the end point contributions are used in the calculation.

The magnitude response is normalized to the highest field value for all geometries considered. The phase is relative and is arbitrarily set to 200 degrees in the quiet zone region. This value allowed for ease in comparison of the phase plots.

Figure 9 shows the normalized magnitude results for the TM case for the corrected PO approach and the FDTD method with reflector and line source geometry. The normalized magnitude of the E_z field versus height above the floor is plotted. There is very little difference between the curves. Note that the two dimensional FDTD results agree within 1 dB with the corrected PO results in the quiet zone region. Figure 10 shows the relative phase of the E_z Field versus height above the floor. The agreement is excellent between both curves in the quiet zone.

Figures 11 and 12 are similar to Figures 9 and 10 and show results for the TE case with the reflector and line source geometry. In Figure 11 the normalized magnitude of the E_y field is plotted versus height above the floor. Again, the agreement between the corrected PO and FDTD results is good. In Figure 12 the relative phase of the E_y field is plotted. Again, the agreement is excellent.

Figures 13 and 14 show the normalized magnitude and phase results for TM polarization for the reflector fed by the line source and by the horn source in free space, and by the horn source in the chamber geometry with absorber over perfectly conducting walls. With the absorber and conducting walls the field values at the floor and the ceiling are zero and are not plotted on the graph. The magnitude values of the field inside the absorber material are shown at Y positions zero + to four feet and 36 to 40 - feet, explaining their low amplitude. With the absorber present the blockage by the feed cover is discernible up to Y position 12'. The expected effect of the absorber in the form of "ripples" upon the planar wavefront in the quiet zone is observed in both the magnitude and phase plots.

Summary and Conclusions

A two dimensional finite difference time domain method for predicting the quiet zone fields of a compact range anechoic cahmber has been presented. Although the approach presented is a two dimensional application of the FDTD method, it produced results which agreed well with a three dimensional corrected PO calculation for a line source and reflector in free space. While the PO approach is limited to conductors in free space, insight into field propagation in a chamber including spillover radiation from the feed horn and feed horn cover blockage of the plane wave as well as

reflections from absorbing materials lining the pit and walls of the chamber can be provided by the FDTD approach.

Future Research

While the results shown in this paper are for a single frequency, application of 2D-FDTD anechoic chamber analysis to wideband signals is straightforward. For narrowband excitation constant values of permeability, permittivity, and conductivity are specified, but for wideband excitation, where these parameters cannot be reasonably approximated as constants, dispersive FDTD formulations may be applied [14].

FDTD is well suited to chamber design. In addition to individually specifying the electrical properties of the absorber at each cell, the location and shape of the absorbing materials can be specified generally as well. Thus effects of absorber placement and material composition can be investigated. Absorber design may be aided by three dimensional FDTD analysis of reflection from individual absorber shapes and material composition.

The shape and material composition of the reflector edge can be modeled using FDTD, and their effects on the quiet zone fields can be computed. The spillover from the feed antenna also can be computed, and the effectiveness of the absorbing materials near the

feed antenna in preventing this energy from reaching the quiet zone can be analyzed. The shape and placement of the absorber on the floor, walls, and ceiling can be modeled, and again the effects of these parameters on the quiet zone fields can be predicted.

References

[1] K. S. Yee, "Numerical solution of initial boundary value problems involving Maxwell's equations in isotropic media," IEEE Trans. Antennas and Propagat., vol. AP-14, pp. 302-307, May 1966.

[2] A. Taflove and M. E. Brodwin, "Numerical solution of steady-state electromagnetic scattering problems using the time-dependent Maxwell's equations," IEEE Trans. Microwave Theory Tech., vol. MTT-23, pp. 623-630, Aug. 1975.

[3] K. S. Kunz and K. M. Lee, "A three-dimensional finite-difference solution of the external response of an aircraft to a complex transient EM environment: Part I - The method and its implementation," IEEE Trans. Electromagnetic Compat., vol. EMC-20, pp. 328-333, May 1978.

[4] K. S. Kunz and K. M. Lee, "A three-dimensional finite-difference solution of the external response of an aircraft to a complex transient EM environment: Part II - Comparison of predictions and measurements," IEEE Trans. Electromagnetic Compat., vol. EMC-20, pp. 333-341, May 1978.

[5] A. Taflove and K. R. Umashankar, "Finite- difference time-domain (FD-TD) modeling of electromagnetic wave scattering and interaction problems," IEEE Antennas and Propagat. Soc. Newsletter, p. 5, Apr. 1988.

[6] C. L. Britt, "Solution of electromagnetic scattering problems using time domain techniques," IEEE Trans. Antennas and Propagat., vol. AP-7, pp. 1191-1192, Sep. 1989.

[7] J. M. Jarem, "Electromagnetic Field Analysis of a Four-Wire Anechoic Chamber," IEEE Trans. Antennas and Propagat., Vol. AP-38, pp. 1835-1842, Nov. 1990.

[8] V. Cable, S. W. Fisher, M. N. Kosma, L. A. Takacs, R. Luebbers, F. Hunsberger, and K. Kunz, "Continuing progress in parallel computational electromagnetics," URSI International Radio Science Meeting, Dallas, Texas, May 6-11, 1990.

[9] I. J. Gupta, K. P. Erickson, and W. D. Burnside, "A method to design blended rolled edges for compact range reflectors," IEEE Trans. Antennas and Propagat., vol. AP-38, pp. 853-861, June 1990.

[10] G. Mur, "Absorbing boundary conditions for finite-difference approximation of the time-domain electromagnetic field equations," IEEE Trans. Electromagnetic Compat., vol. EMC-23, pp. 1073-1077, Nov. 1981.

[11] T. G. Moore, J. Blaschak, A. Taflove, and G. Kriegsman, "Theory and applications of radiation boundary operators," IEEE Trans. Antennas and Propagat., vol. AP-36, pp. 1797-1812, Dec. 1988.

[12] I. J. Gupta and W. D. Burnside, "A Physical Optics Correction for Backscattering from Curved Surfaces," IEEE Trans. Antennas and Propagat., vol. AP-35, pp. 553-561, May 1987.

[13] I. J. Gupta, C.W.I. Pistorius and W.D. Burnside, "An Efficient Method to Compute Spurious End Point Contributions in PO Solutions," IEEE Trans. Antennas and Propagat., vol. AP-35, pp. 1426-1435, Dec. 1987.

[14] R. J. Luebbers, F. P. Hunsberger, K. S. Kunz, R. B. Standler, and M. Schneider "A frequency dependent Finite Difference Time Domain formulation for dispersive materials," IEEE Trans. Electromagn. Compat., vol. EMC-32, pp. 222-227, Aug. 1990.

Figure Titles

Figure 1 Two dimensional FDTD computational cell showing the staggered spatial locations of the electric and magnetic fields for the TE and TM polarizations.

Figure 2 Centerline slice of the low frequency reflector in the NASA Langley anechoic chamber.

Figure 3 Line drawing of 80' by 48' anechoic chamber showing absorber placement, reflector, and horn feed. The sampling locations are indicated by dots.

Figure 4 First problem space geometry showing chamber dimensions (---), placement of reflector and focal point (X), and variable cell border (CB) between the chamber and the outer mesh absorbing boundaries.

Figure 5 Time variation of excitation source is a Gaussian modulated 330 MHz sine wave.

Figure 6 Electric field versus time at quiet zone location (39.5',18') showing the direct source radiation and the reflected wave from the low frequency reflector.

Figure 7 Electric field versus time at quiet zone location (39.5',22') showing the direct source radiation and the reflected wave from the low frequency reflector.

Figure 8 Two Dimensional horn source depicting excitation line source position with a circle and the reflector focal point by an X.

Figure 9 Normalized magnitude of electric field (E_z) versus quiet zone position for the TM polarization for the Reflector and line source in free space.

Figure 10 Relative phase of electric field (E_z) versus quiet zone position for the TM polarization for the Reflector and line source in free space.

Figure 11 Normalized magnitude of electric field (E_y) versus quiet zone position for the TE polarization for the Reflector and line source in free space.

Figure 12 Relative phase of electric field (E_y) versus quiet zone position for the TE polarization for the Reflector and line source in free space.

Figure 13 Normalized magnitude of electric field (E_z) versus quiet zone position for TM polarization for the Reflector fed by the line source and horn in free space, and fed by the horn in the chamber with absorber.

Figure 14 Relative phase of electric field (E_z) versus quiet zone position for TM polarization for the Reflector fed by the line source and horn in free space, and fed by the horn in the chamber with absorber.

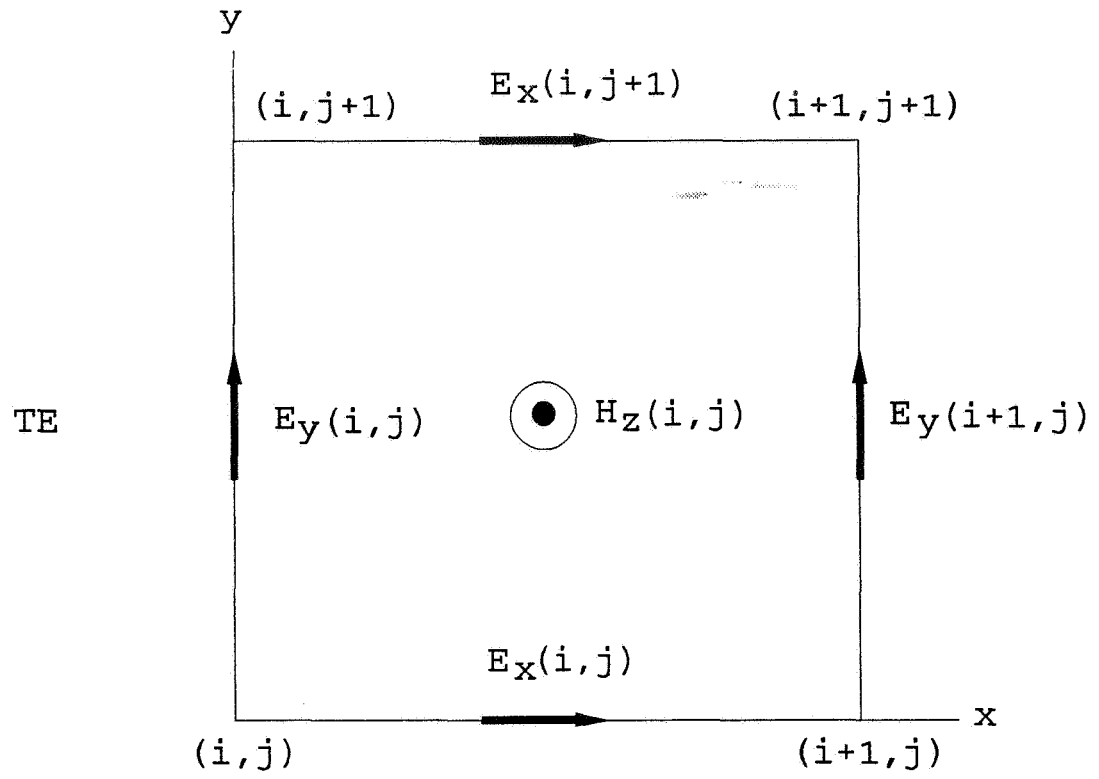
y
(i,j+1)
Ex(i,j+1)
(i+1,j+1)
TE
Ey(i,j)
Hz(i,j)
Ey(i+1,j)
Ex(i,j)
x
(i,j)
(i+1,j)

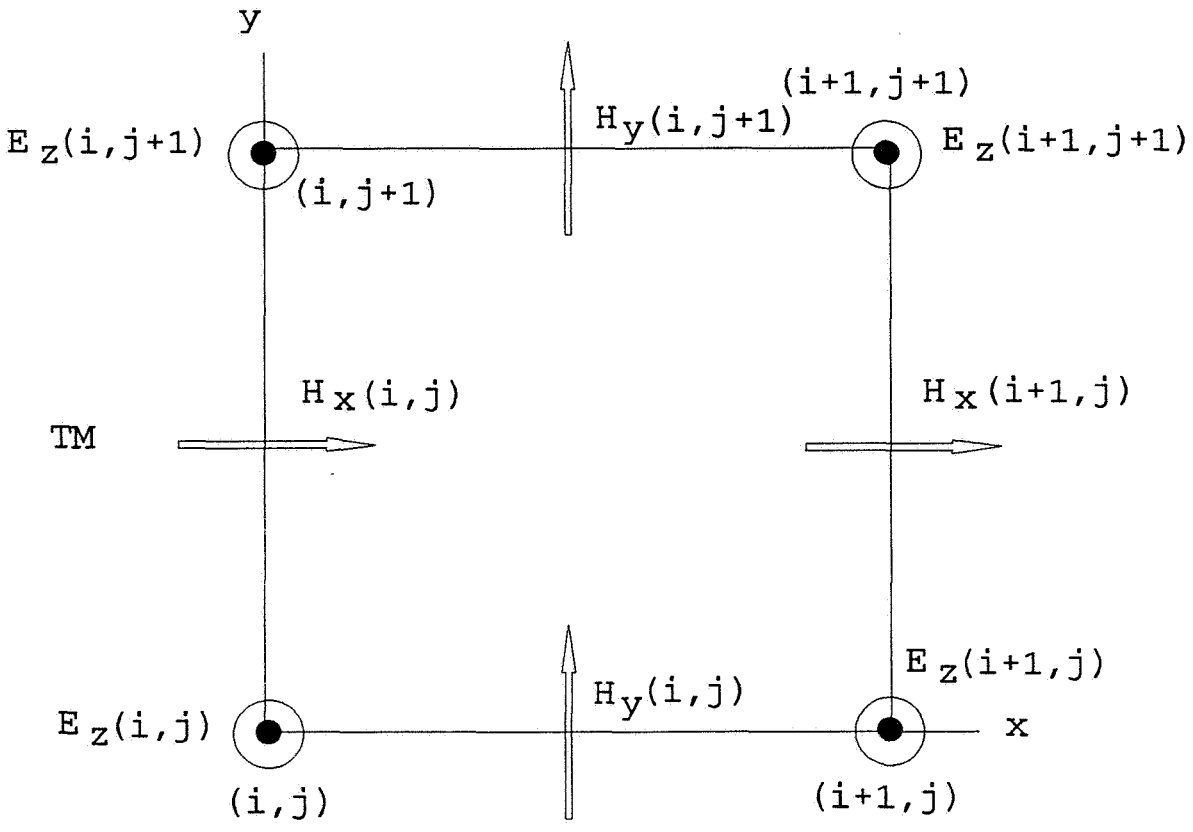
y
(i+1,j+1)
Hy(i,j+1)
Ez(i,j+1)
Ez(i+1,j+1)
(i,j+1)
Hx(i,j)
Hx(i+1,j)
TM
Ez(i+1,j)
Hy(i,j)
Ez(i,j)
x
(i,j)
(i+1,j)

Low Frequency Reflector
Centerline slice

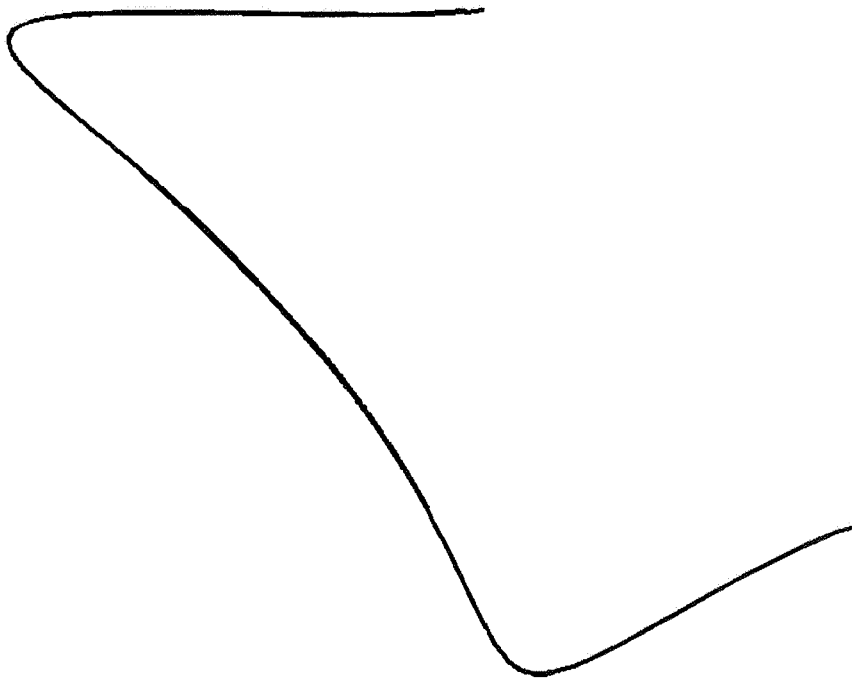

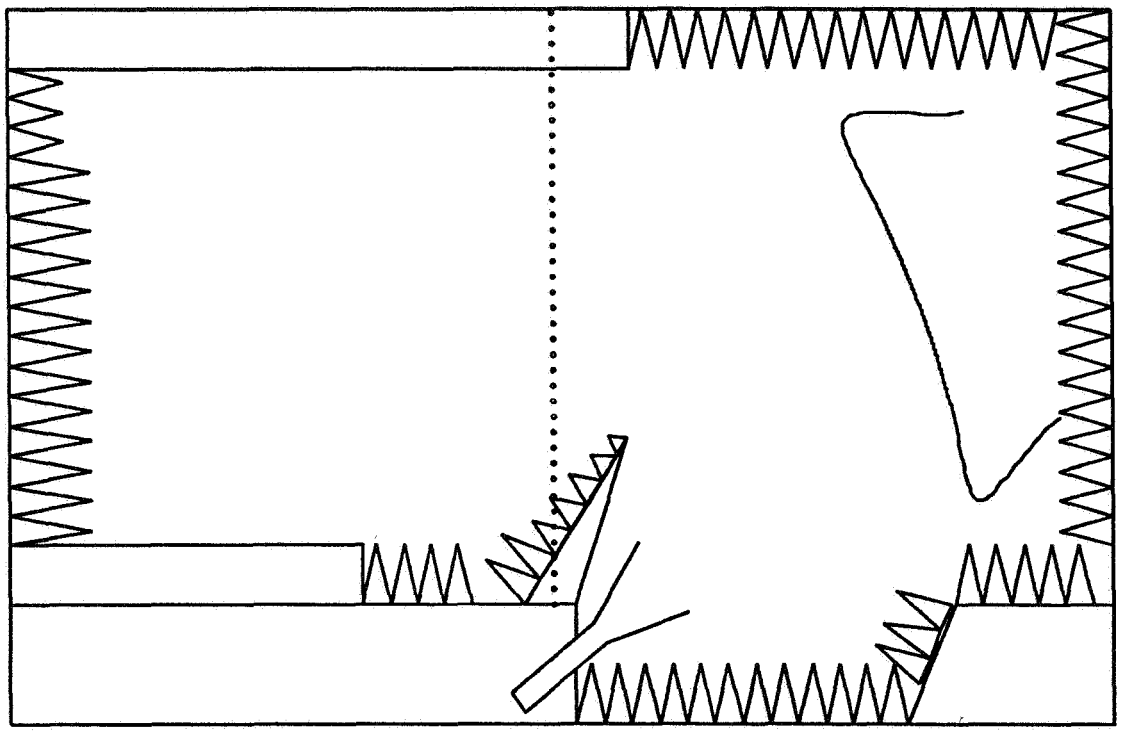

Problem Space Geometry
2D-FDTD

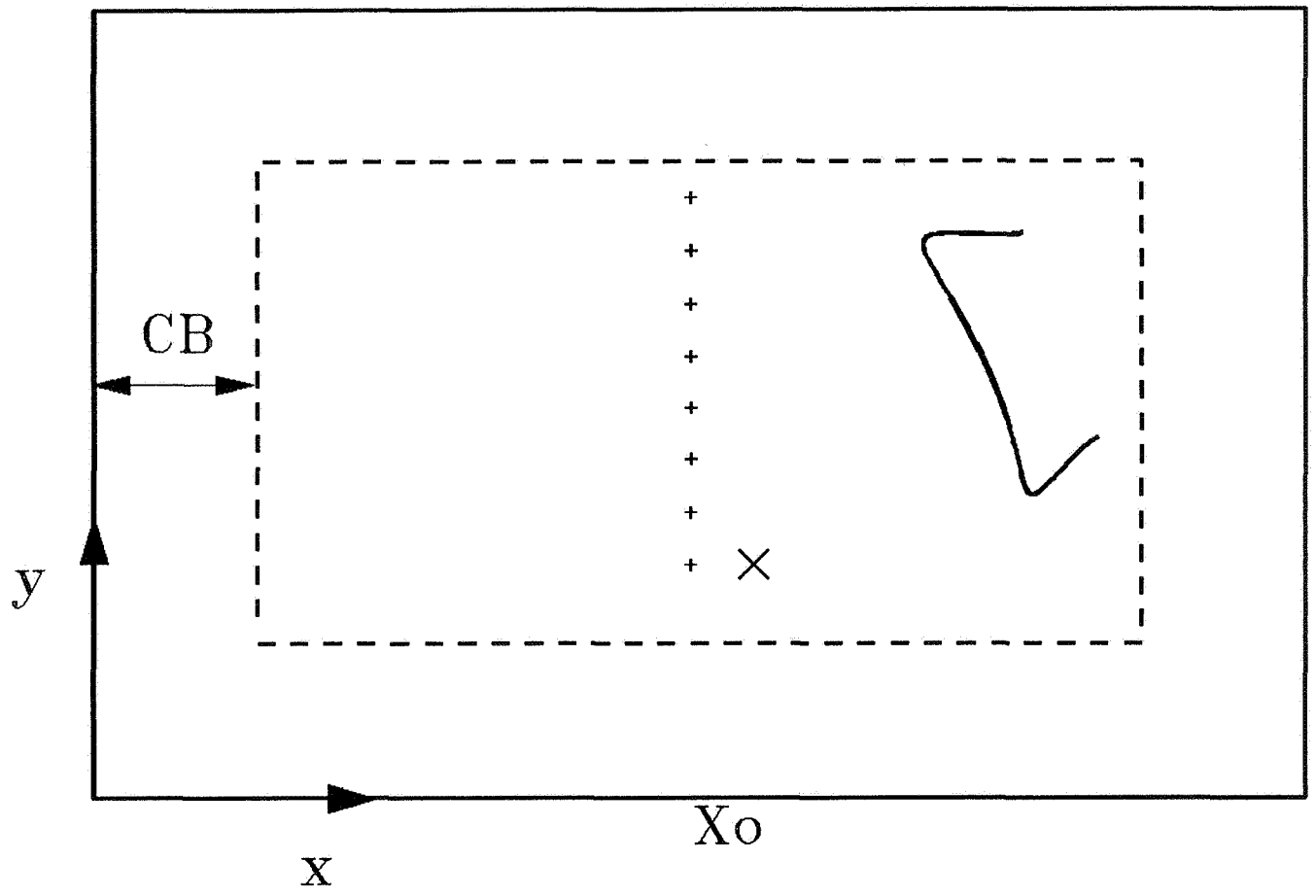

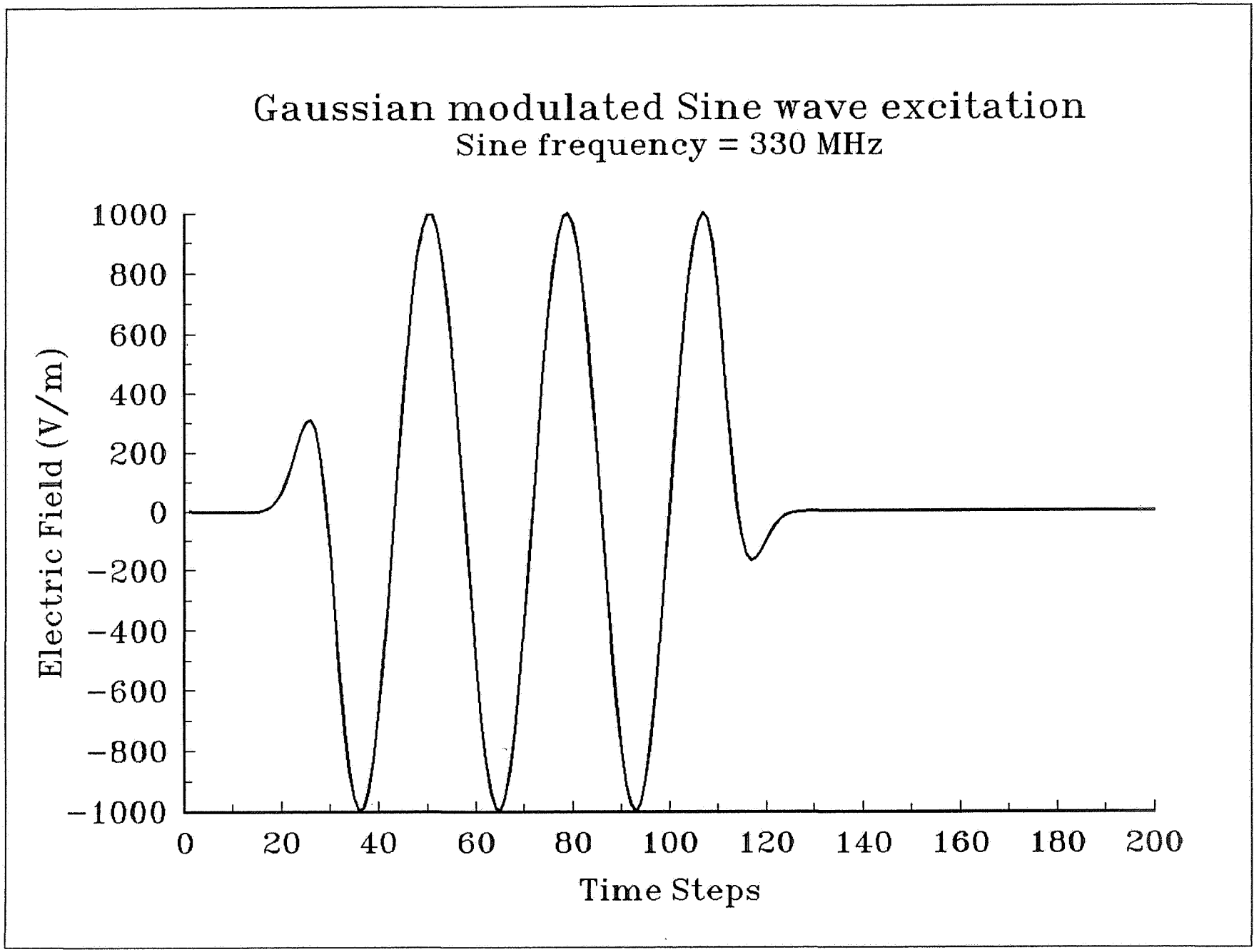
Gaussian modulated Sine wave excitation
Sine frequency = 330 MHz
Electric Field (V/m)
1000
800
600
400
200
0
−200
−400
−600
−800
−1000
0
20
40
60
80
100
120
140
160
180
200
Time Steps

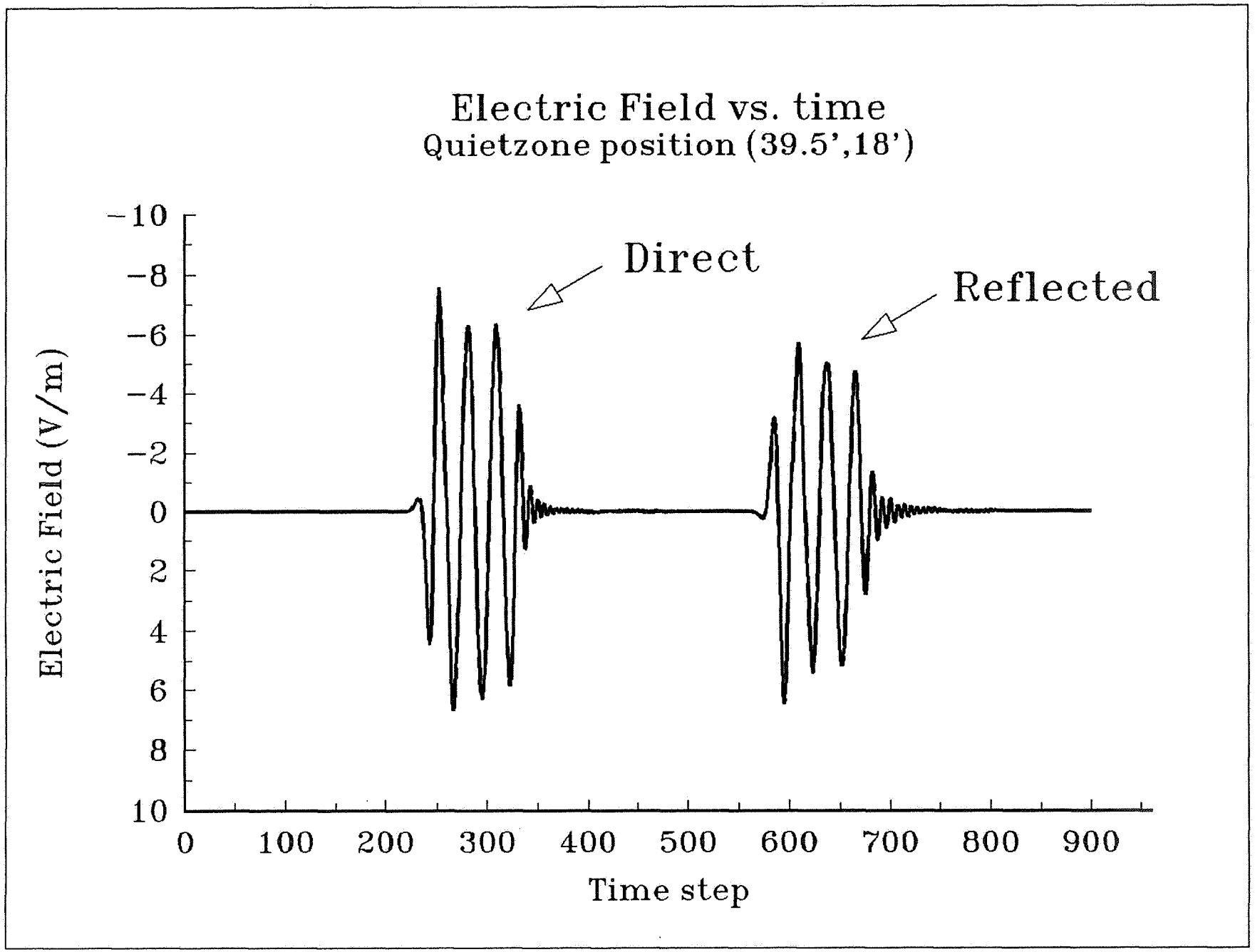
Electric Field vs. time
Quietzone position (39.5',18')
Direct
Reflected
Electric Field (V/m)
−10
−8
−6
−4
−2
0
2
4
6
8
10
0
100
200
300
400
500
600
700
800
900
Time step

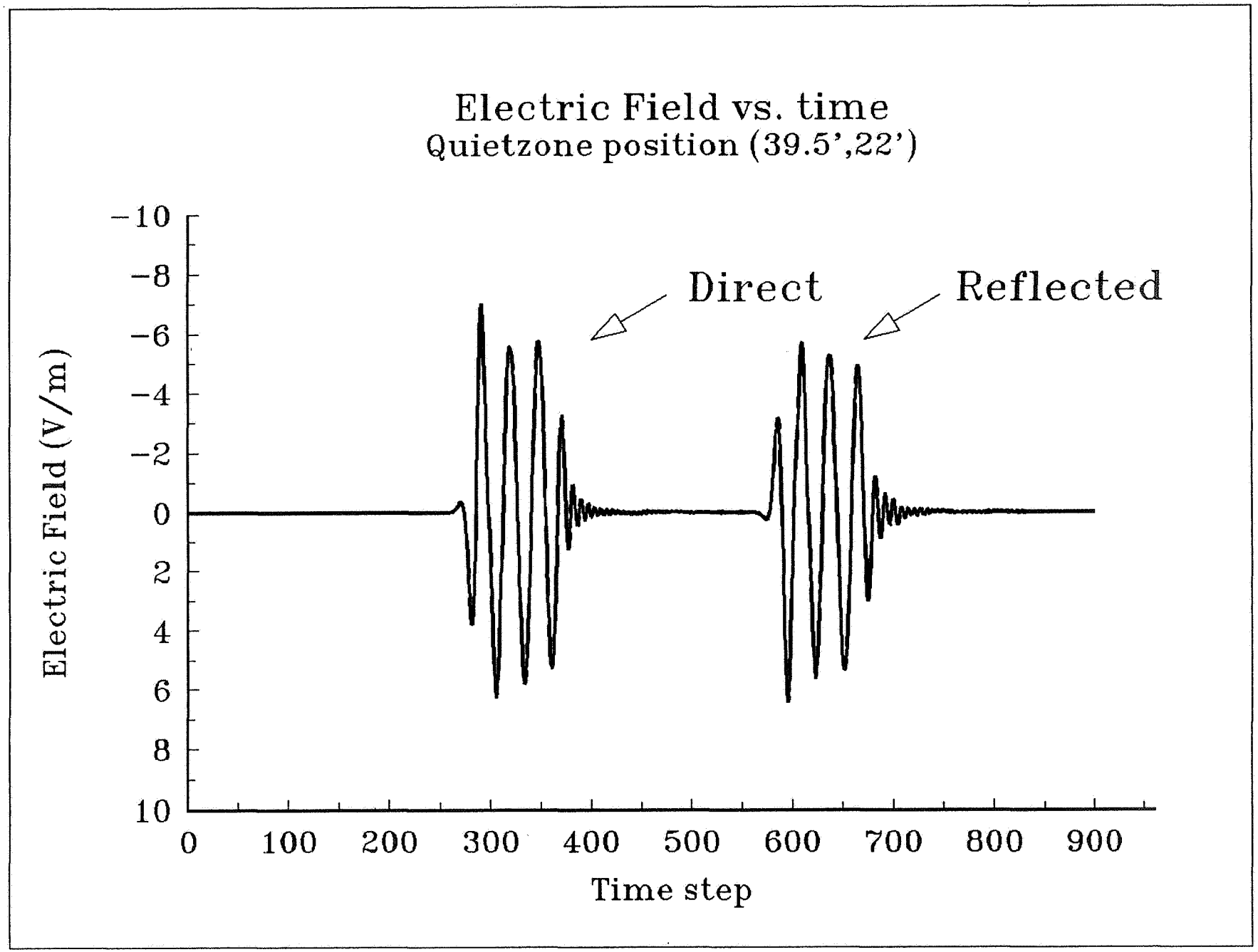
Electric Field vs. time
Quietzone position (39.5',22')
Direct
Reflected
Electric Field (V/m)
-10
-8
-6
-4
-2
0
2
4
6
8
10
0
100
200
300
400
500
600
700
800
900
Time step

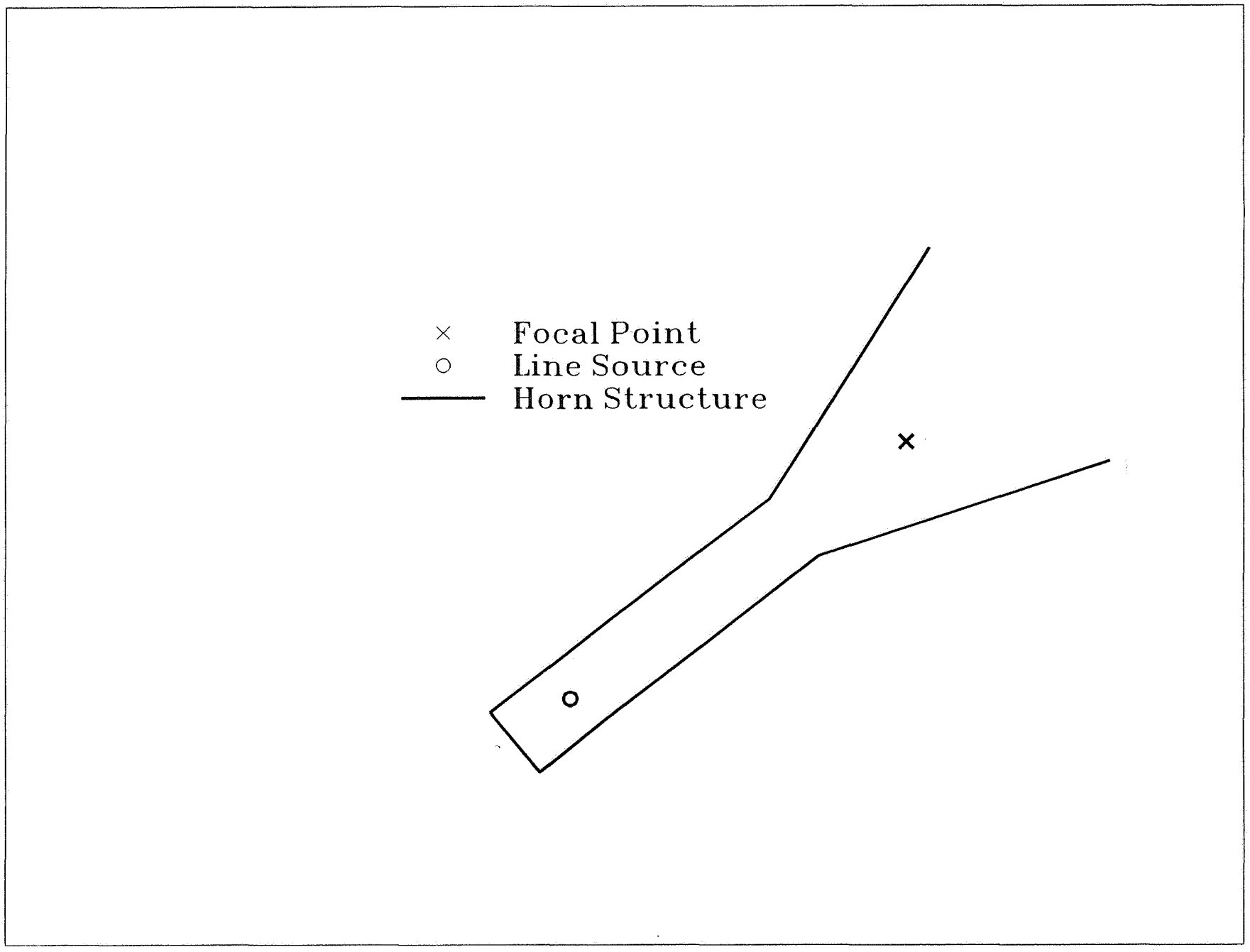
Focal Point
Line Source
Horn Structure

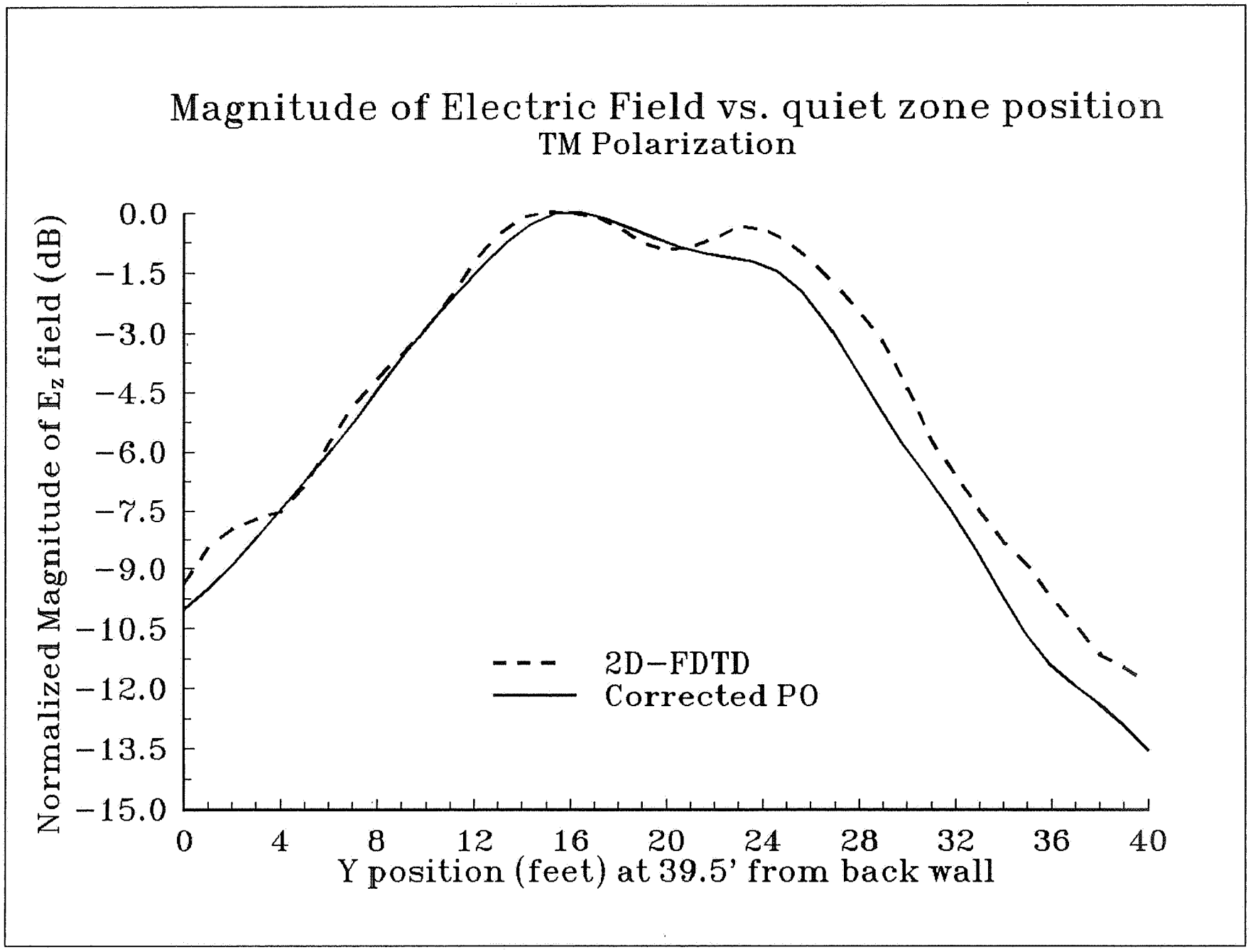
Magnitude of Electric Field vs. quiet zone position
TM Polarization
Normalized Magnitude of E_z field (dB)
0.0
−1.5
−3.0
−4.5
−6.0
−7.5
−9.0
−10.5
−12.0
−13.5
−15.0
0
4
8
12
16
20
24
28
32
36
40
Y position (feet) at 39.5' from back wall
2D−FDTD
Corrected PO

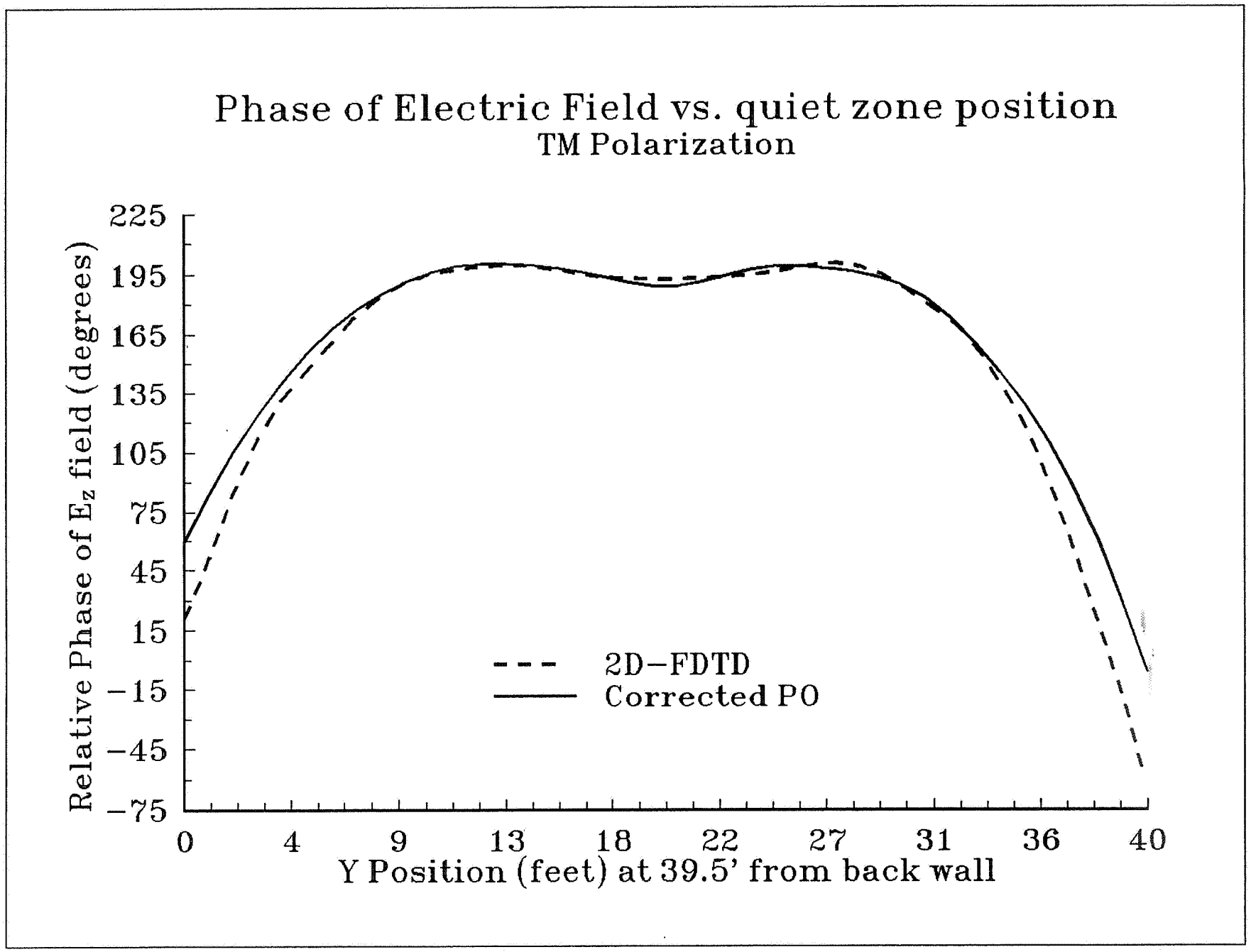
Phase of Electric Field vs. quiet zone position
TM Polarization
Relative Phase of E_z field (degrees)
225
195
165
135
105
75
45
15
−15
−45
−75
0
4
9
13
18
22
27
31
36
40
Y Position (feet) at 39.5' from back wall
2D−FDTD
Corrected PO

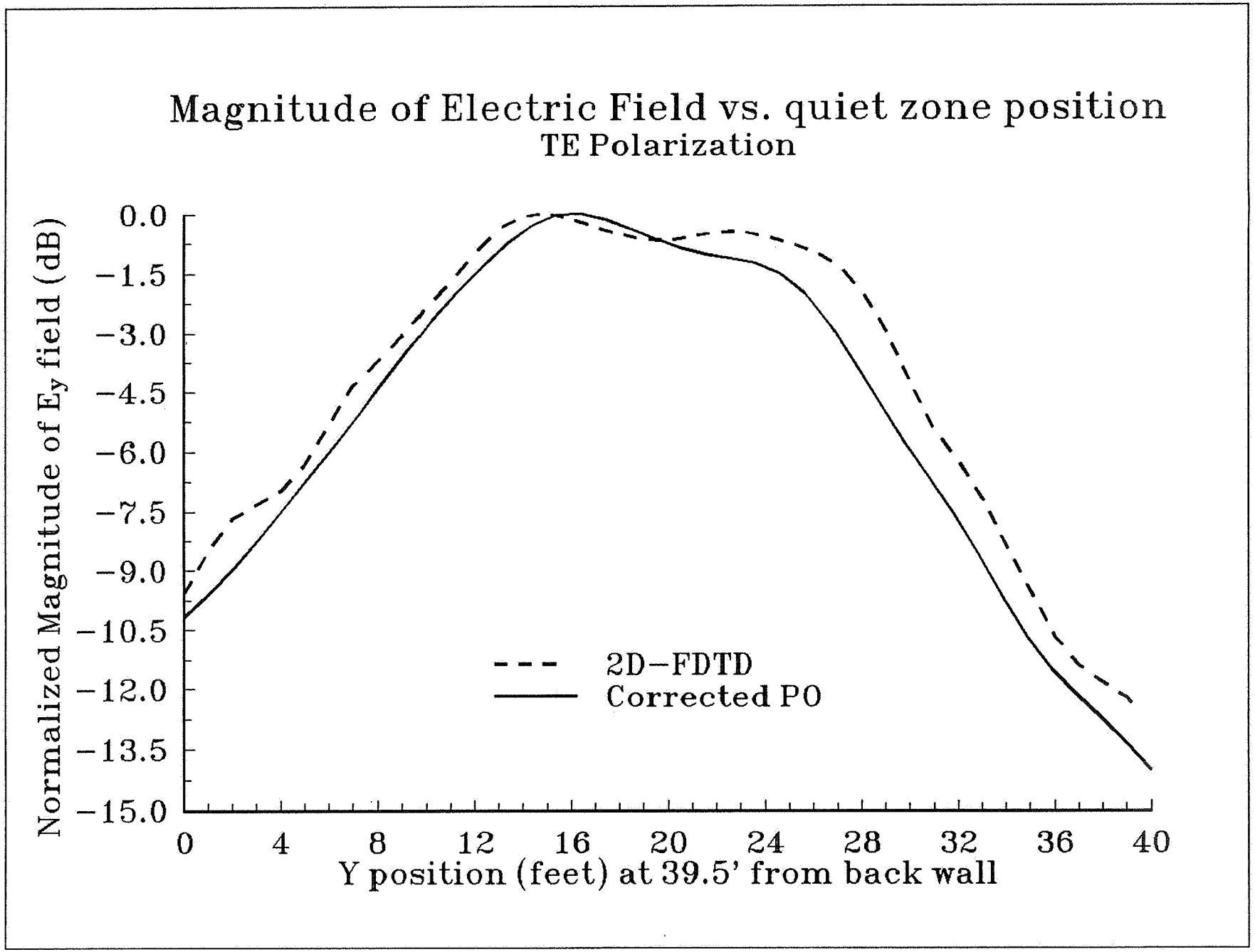
Magnitude of Electric Field vs. quiet zone position
TE Polarization
Normalized Magnitude of Ey field (dB)
0.0
−1.5
−3.0
−4.5
−6.0
−7.5
−9.0
−10.5
−12.0
−13.5
−15.0
0
4
8
12
16
20
24
28
32
36
40
Y position (feet) at 39.5' from back wall
2D−FDTD
Corrected PO

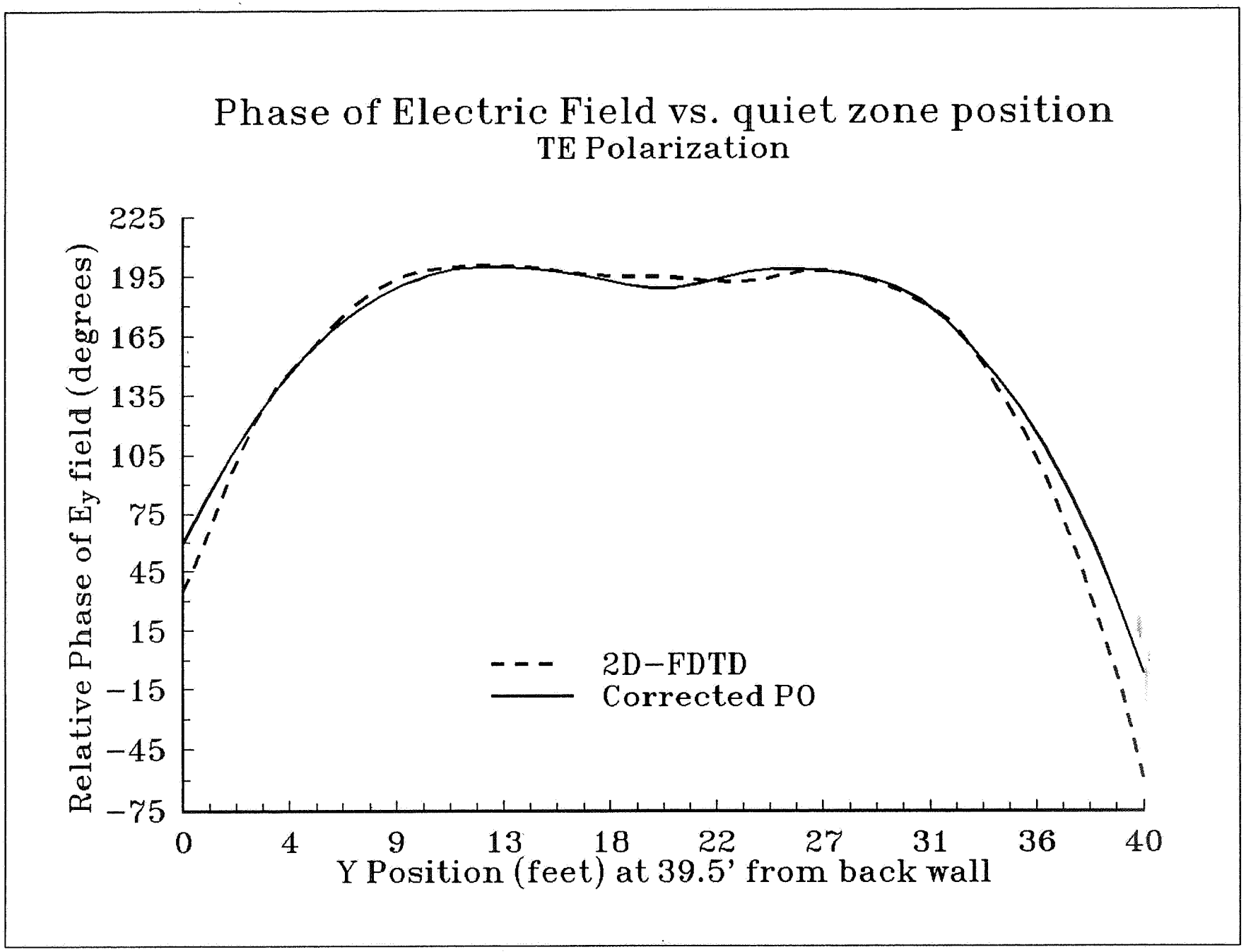
Phase of Electric Field vs. quiet zone position
TE Polarization
Relative Phase of E_y field (degrees)
225
195
165
135
105
75
45
15
−15
−45
−75
0
4
9
13
18
22
27
31
36
40
Y Position (feet) at 39.5' from back wall
2D−FDTD
Corrected PO

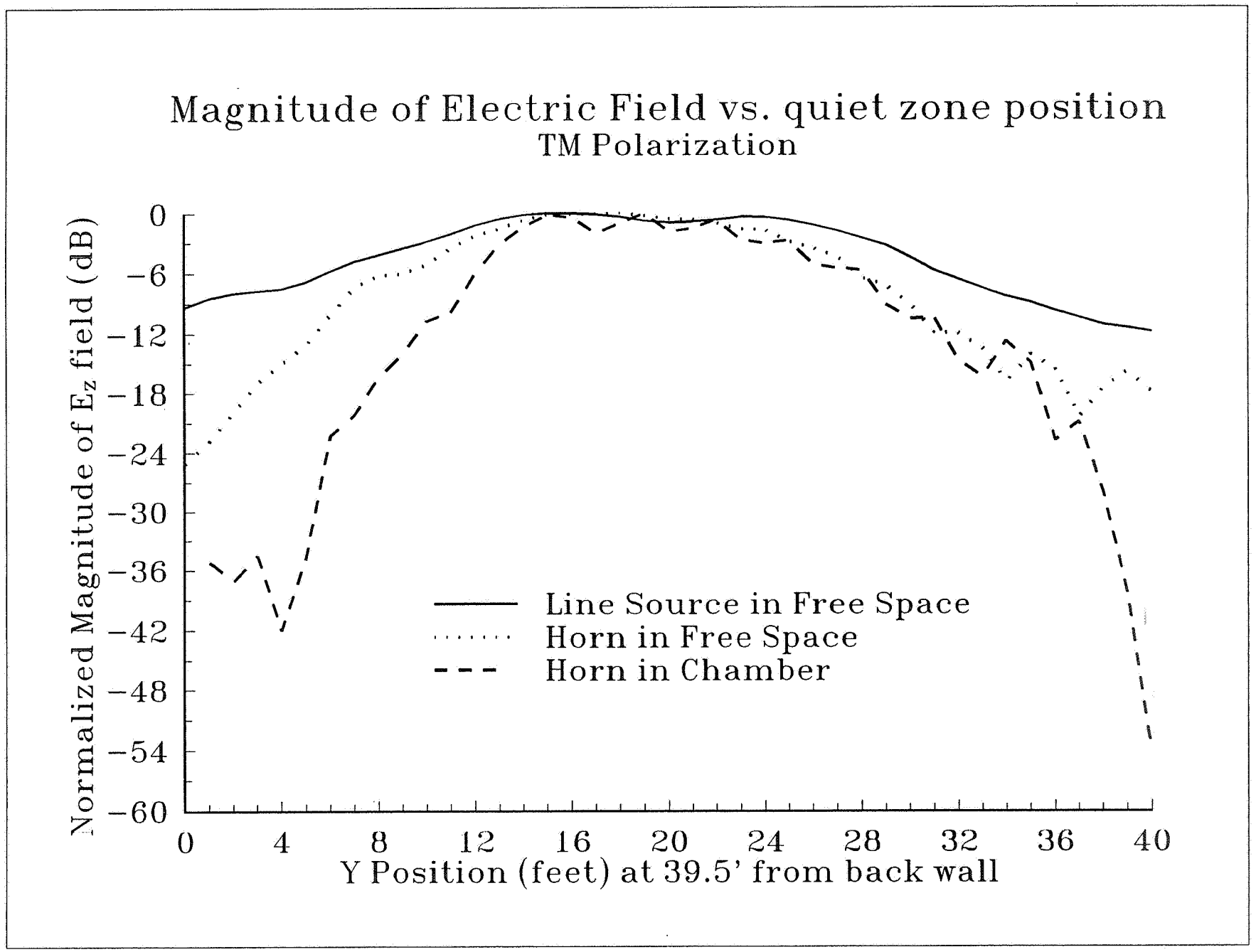
Magnitude of Electric Field vs. quiet zone position
TM Polarization
Normalized Magnitude of E_z field (dB)
0
−6
−12
−18
−24
−30
−36
−42
−48
−54
−60
0
4
8
12
16
20
24
28
32
36
40
Y Position (feet) at 39.5' from back wall
Line Source in Free Space
Horn in Free Space
Horn in Chamber

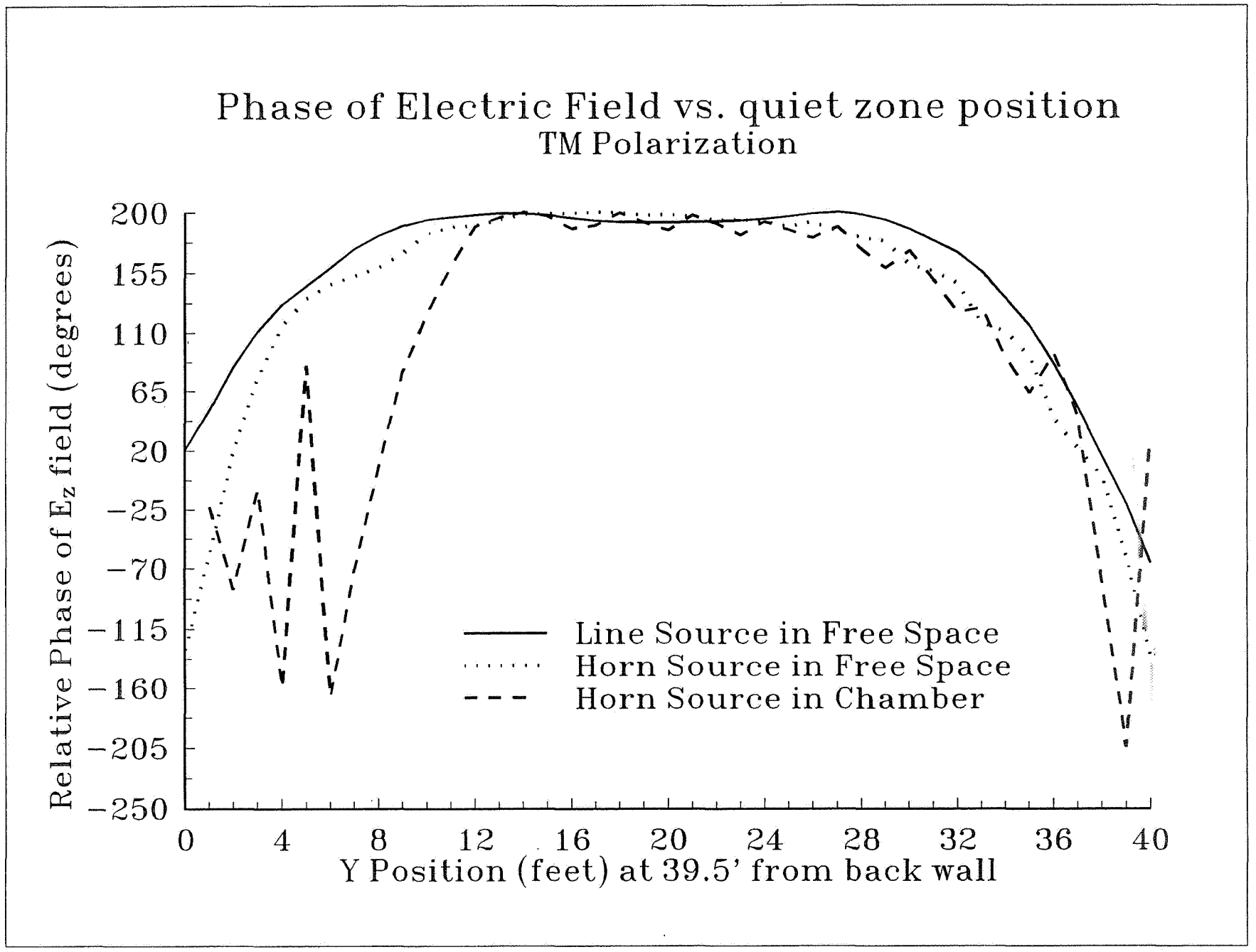
Phase of Electric Field vs. quiet zone position
TM Polarization
Relative Phase of E_z field (degrees)
200
155
110
65
20
−25
−70
−115
−160
−205
−250
0
4
8
12
16
20
24
28
32
36
40
Y Position (feet) at 39.5' from back wall
Line Source in Free Space
Horn Source in Free Space
Horn Source in Chamber